Unified Theory for the Langmuir Probe in a Collisionless Plasma

S. H. Lam

Citation: Physics of Fluids **8**, 73 (1965); doi: 10.1063/1.1761103
View online: http://dx.doi.org/10.1063/1.1761103
View Table of Contents: http://scitation.aip.org/content/aip/journal/pof1/8/1?ver=pdfcov
Published by the AIP Publishing

Unified Theory for the Langmuir Probe in a Collisionless Plasma

S. H. LAM
Gas Dynamics Laboratory, Princeton University, Princeton, New Jersey
(Received 2 June 1964; final manuscript received 3 September 1964)

An asymptotic analysis is presented of the Langmuir-probe problem in a quiescent, collisionless plasma in the limit of large body dimension to Debye length ratio. The structures of the electric potential distribution about spheres and cylinders are analyzed and discussed in detail. It is shown that when the probe potential is smaller than a certain well defined value, there exists no sheath adjacent to the solid surface. At large body potentials, for which a sheath is present, the electric potential distribution is given in terms of several universal functions. Master current-voltage characteristic diagrams are given which exhibit clearly the effects of all the pertinent parameters in the problem. An explicit trapped-ion criterion is presented. The general problem with an arbitrary body dimension to Debye length ratio is qualitatively discussed.

I. INTRODUCTION

THE Langmuir probe is one of the simplest diagnostic tools in the study of ionized gases. The probe is usually a small sphere or a circular cylinder which is placed in the plasma at the point of interest. External circuitry is provided so that the electric potential of the probe can be varied. A plot of the total current flowing between the probe and the plasma versus the probe potential is called the current–voltage characteristic or simply the C–V diagram. Theoretical interests in the Langmuir probe problem are motivated in part by the realization that important information about the plasma can be obtained from the C–V diagram. Moreover, the structure of the electric potential distribution about a Langmuir probe normally exhibits a sheath adjacent to the solid surface, and this plasma-solid surface interaction phenomenon is of sufficient general interest to warrant detailed investigation.

While the Langmuir-probe problem under completely general conditions is quite complicated, the basic physical processes involved were clearly identified by Langmuir[1] himself. Langmuir pointed out that the solid surface, which is generally cold with respect to the plasma temperature, acts as an absorber of the charged particles since they tend to recombine there. Based on the assumption that the plasma is collisionless and the realization that the potential of the probe repels charged particles of one sign and attracts the other, Langmuir gave estimates of the values of the saturation currents for very large positive and negative potentials. He also argued that the natural tendency for a plasma to remain neutral would tend to confine the potential drop to a thin sheath adjacent to the solid surface, and he used the standard Child–Langmuir formula to describe the structure of the sheath. Bohm[2] and later Allen, Boyd, and Reynolds[3] refined Langmuir's analysis. In particular, it was shown that for cold ions and hot electrons the ion saturation current depends on the electron temperature instead of the ion temperature as had been previously believed. Recently, Bernstein and Rabinowitz[4] reformulated the problem by performing a detailed analysis of the orbits of the attracted particles about the probe. The number density of the attracted particles as a function of position and local potential was derived for spherical and cylindrical probes under the assumption that these particles are mono-energetic.

Bernstein and Rabinowitz integrated the resulting governing equation numerically and presented both the C–V diagrams and the potential distributions about the probes for a number of cases. While their formulation is presently the most rigorous and complete one available, their results are difficult to use as is the case of any numerically constructed solution. Much cross-plotting is necessary in order to obtain specific information of interest. In the present paper, we reconsider the collisionless Langmuir probe problem following the formulation of Bernstein and Rabinowitz. We take advantage of the fact that in practical cases the ratio of probe radius to Debye length is very large and we perform an asymptotic analysis in this limit. Almost all of the previously known theories[1–4] can be shown to be special cases of the present unified theory.

[1] I. Langmuir, *The Collected Works of Irving Langmuir*, edited by C. Suits (Pergamon Press, Inc., New York, 1961), Vol. 4, pp. 23–132.

[2] D. Bohm, in *Characteristics of Electrical Discharges in Magnetic Fields*, edited by A. Guthrie and R. Wakerling (McGraw-Hill Book Company, Inc., New York, 1949), Chap. 3.

[3] J. E. Allen, R. L. F. Boyd and P. Reynolds, Proc. Phys. Soc. (London) **B70**, 297 (1956).

[4] I. Bernstein and I. Rabinowitz, Phys. Fluids **2**, 112 (1959).

II. STATEMENT OF THE PROBLEM

The basic equation governing the electric potential is

$$\nabla^2\phi = -4\pi e(ZN_i - N_e), \tag{2.1}$$

where ϕ is the electric potential, e is the absolute magnitude of the charge of an electron (4.8×10^{10} esu), Z is the charge number of the ions, and N_i and N_e are the number densities of the ions and electrons, respectively. For a spherically symmetric problem, the independent variable is simply r. We now define

$$\chi = -\frac{e\phi}{KT_e}, \quad n_i = \frac{ZN_i}{N_\infty}, \quad n_e = \frac{N_e}{N_\infty},$$
$$z = \frac{R}{r}, \quad \xi_e = \frac{R}{h_e}, \quad h_e = \left(\frac{KT_e}{4\pi N_\infty e^2}\right)^{\frac{1}{2}}, \tag{2.2}$$

where K is the Boltzmann constant (1.38047×10^{-16} ergs/°K), T_e is the electron temperature, N_∞ is the undisturbed electron number density, R is the radius of the spherical probe, and h_e is the electron Debye length. In these variables, Eq. (2.1) becomes

$$\frac{z^4}{\xi_e^4}\frac{d^2\chi}{dz^2} = n_i - n_e. \tag{2.3}$$

The number ξ_e is a parameter specifying the probe size. Subscript p always denotes conditions on the probe surface. For example, the value of χ on the probe surface is denoted by χ_p.

Equation (3.2) is to be supplemented by other equations governing the number density distributions n_i and n_e. For continuum plasmas, these would be the equations stating the conservation of mass and the diffusion velocities.[5-7] For a collisionless plasma, the number density distributions, n_i and n_e, are to be calculated by a detailed analysis of the trajectories of the particles. Under the assumption of mono-energetic ions, Bernstein and Rabinowitz[4] give the following expression for n_i:

$$n_i = \tfrac{1}{2}\left(1 + \frac{\chi}{\beta}\right)^{\frac{1}{2}} \pm \tfrac{1}{2}\left[1 + \frac{\chi}{\beta} - jz^2\left(1 + \frac{1}{\beta}\right)^{\frac{1}{2}}\right]^{\frac{1}{2}}, \tag{2.4}$$

where the plus and minus signs in Eq. (2.4) are to be used for $z \leq z_0$ and $z \geq z_0$, respectively. The dimensionless parameters β and j are defined by:

$$\beta = E_i/ZKT_e \tag{2.5}$$

$$j = I_i/\pi R^2 N_\infty[2(E_i + ZKT_e)/m_i]^{\frac{1}{2}} \tag{2.6}$$

and E_i is the energy of the ions [see Eq. (6.7) later which relates E_i with T_i], I_i is the total number of positive charges absorbed by the probe per second and m_i is the mass of an ion. The point $z = z_0$ is defined as the position where the solution curve $\chi(z)$ osculates the line

$$1 + \frac{\chi}{\beta} - jz^2\left(1 + \frac{1}{\beta}\right)^{\frac{1}{2}} = 0. \tag{2.7}$$

By performing a similar analysis of orbits following Bernstein and Rabinowitz, the electron density distribution is found to be

$$n_e = \exp(-\chi)\left\{1 - \frac{1}{2g(0)}\left[g(\chi_p - \chi) - (1 - z^2)^{\frac{1}{2}} g\left(\frac{\chi_p - \chi}{1 - z^2}\right)\exp\left(z^2\frac{\chi_p - \chi}{1 - z^2}\right)\right]\right\}, \tag{2.8}$$

where $g(\lambda)$ is defined as

$$g(\lambda) = \int_\lambda^\infty \xi^{\frac{1}{2}} e^{-\xi}\, d\xi. \tag{2.9}$$

Note that $g(\lambda) \ll 1$ if $\lambda \gg 1$. In arriving at Eq. (2.8), the electron distribution function far away from the probe is assumed Maxwellian. The details of the derivation of Eq. (2.8) are presented in Appendix I. Note that at $z = 1$, $\chi = \chi_p$, Eq. (2.8) gives $n_e = \frac{1}{2}e^{-\chi_p}$.

Equations (2.3), (2.4), and (2.8) together constitute the governing set of equations for our problem. The boundary conditions are

$$\chi(z = 0) = 0, \tag{2.10a}$$

$$\chi(z = 1) = \chi_p. \tag{2.10b}$$

The value of j which appears in Eq. (2.4) is not known *a priori*, but must be found by fitting the boundary conditions. Formally, it is desired to find a function

$$\chi = \chi(z; \xi_e, \beta, j, \chi_p) \tag{2.11}$$

satisfying Eqs. (2.3), (2.4), (2.8) and (2.10a). By evaluating Eq. (2.11) at $z = 1$ and applying boundary condition Eq. (2.10b), we have

$$\chi_p = (1; \xi_e, \beta, j, \chi_p) \tag{2.12}$$

which relates j and χ_p and is therefore the ion C–V characteristic. The desired potential distribution $\chi(z)$, for a given set of parameters ξ_p, β, and χ_p, is obtained by inserting the proper value for j from Eq. (2.12) into Eq. (2.11). A discussion of whether the problem is properly posed is given in Sec. IX.

In most existing works, Eq. (2.8) is approximated by

$$n_e = e^{-\chi}, \tag{2.13}$$

[5] C. H. Su and S. H. Lam, Phys. Fluids **6**, 1479 (1963).
[6] I. Cohen, Phys. Fluids **6**, 1492 (1963).
[7] S. H. Lam, AIAA J. **2**, 256 (1964).

and can be justified if attention is confined to the $\chi_p \gg 1$ case. From Eq. (2.8), we see that the percentage error of Eq. (2.13) is $O[g(\chi_p)]$ except when $\chi \sim \chi_p$. However, for $\chi \sim \chi_p \gg 1$, n_e becomes negligible in comparison to n_i. Bernstein and Rabinowitz solved Eqs. (2.3), (2.4), and (2.13) numerically (using a different nondimensional scheme) for the following range of parameters: $\xi_e \lesssim 15$, $0.10 \geq \beta \geq 0$, $480 \geq j\xi_e^2(1+\beta)^{\frac{1}{2}} \geq 80$. Hence their results are useful for moderate values of ξ_e. The present paper concerns itself mainly with the asymptotic solutions for arbitrary but finite values of β in the limit of $\xi_e \gg 1$. Therefore the results obtained here cover a different region in the parameter space, but sufficient overlap exists to allow comparisons. The limiting case of $\xi_e \ll 1$ is briefly treated in Sec. IX.

The assumption of $\xi_e \gg 1$ is normally a realistic one. Since we are dealing with a collisionless model, the ordering of characteristic lengths is $l \gg R \gg h_e$ where l is the characteristic mean free path of the charged particles.

III. MODERATELY NEGATIVE PROBE POTENTIALS

In the limit of $\xi_p \gg 1$, Eq. (2.3) becomes

$$n_i = n_e + O(\xi_e^{-2}) \tag{3.1}$$

Equation (3.1) relates χ and z and is generally referred to as the quasineutral approximation. Evaluating Eq. (3.1) at $z = 1$ where $\chi = \chi_p$, and using Eqs. (2.4) and (2.8) for n_i and n_e, respectively, we can solve for j to obtain the following expression

$$j = \frac{e^{-\chi_p}}{(1+\beta)^{\frac{1}{2}}}\{2(\beta+\chi_p)^{\frac{1}{2}} - \beta^{\frac{1}{2}}e^{-\chi_p}\}, \tag{3.2}$$

which is the ion C–V characteristic. In order to justify Eq. (3.1) as the correct quasineutral solution, we must check the order of magnitude of $\xi_e^{-2}z^4\, d^2\chi/dz^2$ as $\xi_e \to \infty$. A detailed study indicates that these quasineutral solutions have the property that for a fixed value of β the value of $(d^2\chi/dz^2)_{z=1}$ tends to infinity as χ_p increases toward a certain value $\tilde{\chi}_p(\beta)$, and that no continuous solution exists for $\chi_p > \tilde{\chi}_p(\beta)$. The validity of Eq. (3.2), therefore, terminates at $\chi_p = \tilde{\chi}_p(\beta)$. *Thus for $\chi_p < \tilde{\chi}_p(\beta)$, the plasma is quasineutral throughout and no sheath is present even adjacent to the probe surface.* The exact values for $\tilde{\chi}_p(\beta)$ are given by the value of χ_p at which j from Eq. (3.2) is a maximum. Taking the derivative of Eq. (3.2) with respect to χ_p and setting $dj/d\chi_p$ to zero, we obtain an implicit equation for $\tilde{\chi}_p(\beta)$:

$$\tilde{\chi}_p = \tfrac{1}{2} - \beta[1 - (1 + \tilde{\chi}_p/\beta)^{\frac{1}{2}} \exp(-\tilde{\chi}_p)]. \tag{3.3}$$

Table I gives $\tilde{\chi}_p(\beta)$ for several values of β. Equation (3.2) is, therefore, the appropriate asymptotic (in the $\xi_p \to \infty$ sense) C–V relation for $\tilde{\chi}_p > \chi_p \geq 0$. Note that at $\chi_p = 0$, we have the trivial solution $\chi = 0$, $j = [\beta/(1+\beta)]^{\frac{1}{2}}$. From Eqs. (2.5) and (2.6), we have

$$I_i = \pi R^2 N_\infty (2E_i/m_i)^{\frac{1}{2}}, \qquad (\chi_p = 0), \tag{3.4}$$

which is simply the random ion current collected by the probe in the absence of electric fields.

IV. HIGHLY NEGATIVE PROBE POTENTIAL CASE

While no formal analytical difficulty is expected in using Eq. (2.8) for the analysis which follows, we shall for the sake of simplicity adopt Eq. (2.13) and thereby limit our attention to highly negative probe potentials. A brief outline on how to handle the intermediate probe-potential case using Eq. (2.8) is given in Sec. V.

For highly negative probe potentials, the electric disturbances about the probe can be divided into a quasineutral region far from the probe and a sheath region adjacent to the probe. Two transitional layers exist which together serve to join the quasineutral region with the sheath region.

Quasineutral Region

In the limit of $\xi_e \gg 1$, Eq. (2.3) again yields

$$n_i = n_e + O(\xi_e^{-2}). \tag{4.1}$$

Using Eqs. (2.4) and (2.13) and simplifying, we obtain

$$z^2 = \frac{4e^{-\chi}}{j}\left(\frac{\beta}{1+\beta}\right)^{\frac{1}{2}}\left[\left(1+\frac{\chi}{\beta}\right)^{\frac{1}{2}} - e^{-\chi}\right] \tag{4.2}$$

which gives z as an explicit function of χ, j, and β. This solution curve osculates with the line given by Eq. (2.7) at $\chi = \chi_0$, $z = z_0$. By simple algebra we

TABLE I. The limits of validity for the quasineutral, moderately negative, probe potential analysis.

β	$\beta \ll 1$	0.1	0.5	1.0	2.0	5.0	10.0	∞
$\tilde{\chi}_p$	$\frac{1}{2}[1 + \beta(2\beta/e)^{\frac{1}{2}} - O(\beta)]$	0.54	0.44	0.33	0.21	0.10	0.05	0.00
$j(\tilde{\chi}_p)$	$0.86[1 - (\beta/2e)^{\frac{1}{2}} + O(\beta)]$	0.79	0.78	0.81	0.86	0.92	0.96	1.0

TABLE II. Location of the osculating point.

β	$\beta \ll 1$	0.1	0.5	1.0	2.0	5.0	10.0	∞
χ_0	$3\beta[1 - 8\beta + O(\beta^2)]$	0.18	0.40	0.49	0.57	0.63	0.66	ln2
$j^{\frac{1}{2}} z_0$	$2\beta^{\frac{1}{2}}[1 - \frac{13}{4}\beta + O(\beta^2)]$	0.919	1.02	1.03	1.02	1.01	1.01	1.0

find the following equations for χ_0 and z_0:

$$\chi_0(\beta) = \beta(4e^{-2\chi_0} - 1),$$
$$jz_0^2 = \left(\frac{\beta}{1+\beta}\right)^{\frac{1}{2}}\left(1 + \frac{\chi_0}{\beta}\right).$$

Table II shows χ_0 and z_0 for various values of β. Note the rapid variation of $j^{\frac{1}{2}}z_0$ with β when $\beta \ll 1$.

Equation (4.2) gives the potential distribution $\chi(z)$ in the quasineutral region. However, this quasineutral curve has the property that $d\chi/dz$ and $d^2\chi/dz^2$ tends to infinity at a certain value of $z = z_1$ (see Fig. 1). For $z < z_1$, the quasineutral curve is double-valued and becomes single-valued only at $z = z_1$. Locating (χ_1, z_1) by standard methods, we find

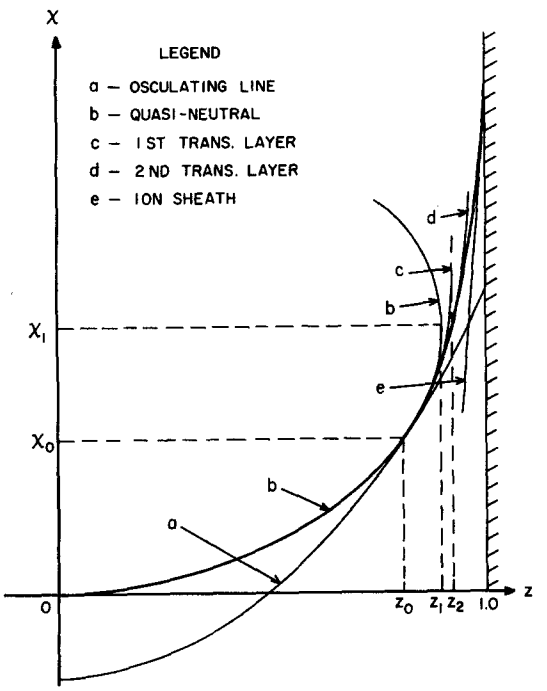

FIG. 1. Qualitative structure of $\chi(z)$ for $\chi_p \gg 1$; $\xi_e \gg 1$.

$$\chi_1 = \tfrac{1}{2} + 2[\beta(\chi_1 + \beta)]^{\frac{1}{2}}e^{-\chi_1} - \beta,$$
$$z_1^2 = \frac{4e^{-\chi_1}}{j(1+\beta)^{\frac{1}{2}}}[(\chi_1 + \beta)^{\frac{1}{2}} - \beta^{\frac{1}{2}}e^{-\chi_1}]. \tag{4.3}$$

Table III shows χ_1 and $z_1 j^{\frac{1}{2}}$ for various values of β. Note that $z_1 j^{\frac{1}{2}}$ is a function of β only and is always of $O(1)$. Also, we see that $\chi_1 > \chi_0$ and $z_1 > z_0$ except for $\beta = \infty$.

The quasineutral curve given by Eq. (4.2) is therefore valid for $z_1 > z \geq 0$, $\chi_1 > \chi \geq 0$ and its accuracy is $O(\xi_e^{-2})$. Near (χ_1, z_1) this curve fails locally as a solution and a transitional layer analysis is needed there.

The First Transitional Layer

We now proceed to expand the right-hand side of Eq. (2.3) about the point (χ_1, z_1). For $\beta \neq \infty$, we have

$$n_i - e^{-\chi} \cong A(\chi - \chi_1)^2 + Bj^{\frac{1}{2}}(z - z_1), \tag{4.4a}$$

where $A(\beta)$ and $B(\beta)$ are constants and are presented in Table IV.

For $\beta = \infty$, the proper expansion is, instead of Eq. (4.4a),

$$n_i - e^{-\chi} \cong A_\infty(\chi_1 - \chi) + B_\infty(z_1 - z)^{\frac{1}{2}}, \tag{4.4b}$$

where A_∞ and B_∞ are of $O(1)$. This limiting case requires a separate analysis. From this point on we assume that β is $O(1)$ unless otherwise stated.

In order to study the detailed structure of the solution $\chi(z)$ near (χ_1, z_1), we introduce new, scaled variables as follows:

$$\chi = \chi_1(\beta) + \left[\frac{(z_1 j^{\frac{1}{2}})^4 B^2}{jA^3\xi_e^2}\right]^{1/5} Y(y),$$
$$z = z_1(j, \beta) + \left[\frac{(z_1 j^{\frac{1}{2}})^8}{j^{9/2}AB\xi_e^4}\right]^{1/5} y, \tag{4.5}$$

TABLE III. Location of the first transitional layer and the value of j_m.

β	$\beta \ll 1$	0.1	0.5	1.0	2.0	5.0	10.0	∞
χ_1	$\frac{1}{2}[1 + 2(2\beta/e)^{\frac{1}{2}} + O(\beta)]$	0.68	0.75	0.75	0.74	0.72	0.71	ln2
$j^{\frac{1}{2}} z_1$	$1.31[1 - \frac{1}{2}(2\beta/e)^{\frac{1}{2}} + O(\beta)]$	1.18	1.10	1.07	1.04	1.02	1.01	1.0
j_m	1.72	1.40	1.21	1.14	1.08	1.04	1.02	1.0

TABLE IV. The values of A and B for Eq. (4.4a).

β	0	0.1	0.5	1.0	2.0	5.0	10.0
A	.606	.561	.681	.894	1.34	2.73	5.24
B	.925	1.10	1.50	1.99	2.94	5.80	10.3

where $z_1 j^{\frac{1}{2}}$ is a function of β only and is given in Table III. Using Eq. (4.5) in Eq. (2.3) and with the aid of Eq. (4.4a), we have, in the limit of $\xi_p \to \infty$

$$d^2Y/dy^2 = Y^2 + y. \tag{4.6}$$

In deriving Eq. (4.6), both Y and y are assumed to be $O(1)$. The error in Eq. (4.6) is $O(\xi_e^{-4/5})$. The boundary condition for Y is that as $y \to -\infty$, Y must match smoothly with the quasineutral curve locally given by

$$\lim_{y\to-\infty} Y = -(-y)^{\frac{1}{2}}, \tag{4.7}$$

and thus Eq. (4.7) is the required behavior for Y as y tends to $-\infty$ (this is standard boundary layer technique, used extensively in fluid mechanics). This boundary condition alone is sufficient to render the solution $Y(y)$ unique; and hence $Y(y)$ is a universal function. This function has been computed numerically and it is found that as $y \to y_2 = 3.45$, Y tends to infinity. Analytically, the behavior near $y = y_2$ is

$$Y = \frac{C}{(y - y_2)^2} + \frac{D}{(y - y_2)} + \cdots, \tag{4.8}$$

where $C = 6.0$ and $D = \frac{1}{6}$. Note that y_2, C, D are universal constants.

The structure of the first transitional layer is also plotted schematically in Fig. 1. It is clear that the analysis above fails locally at $y = y_2$ where Y is no longer of $O(1)$ as assumed. A second transitional layer is found to exist at $y = y_2$ and a separate analysis is required.

The Second Transitional Layer

In terms of z, the second transitional layer is located at $z = z_2$ where

$$z_2 = z_1(\beta, j) + y_2\left[\frac{(z_1 j^{\frac{1}{2}})^8}{j^{9/2}AB\xi_e^4}\right]^{1/5}. \tag{4.9}$$

We also identify z_2 as the edge of the sheath region. Since in general $z_1 j^{\frac{1}{2}} = O(1)$, let us define a new parameter j_m by

$$z_2 = (j_m/j)^{\frac{1}{2}}, \tag{4.10}$$

so that

$$j_m^{\frac{1}{2}} = z_1 j^{\frac{1}{2}} + y_2\left[\frac{(z_1 j^{\frac{1}{2}})^8}{j^2 AB\xi_e^4}\right]^{1/5}. \tag{4.11}$$

For $\xi_e \gg 1$, we have $(j_m)^{\frac{1}{2}} \cong j^{\frac{1}{2}} z_1$, and we see that j_m is primarily a function of β only and is therefore also given in Table III. Since the probe surface is located at $z = 1$, we must require $z_2 \leq 1$. In other words,

$$j \geq j_m. \tag{4.12}$$

Hence, $j_m(\beta)$ is the minimum value of j permissible in the highly negative probe problem. Note that $j_m(\beta)$ is always greater than or equal to the maximum value of j attainable in the moderately negative probe problem (compare Tables I and III).

Now, let us introduce a new, scaled independent variable t by

$$z = z_2 + t/j\xi_e. \tag{4.13}$$

Without any assumption or transformation on χ, Eq. (2.3) becomes

$$j_m^2 \frac{d^2\chi}{dt^2} = \tfrac{1}{2}\left(1 + \frac{\chi}{\beta}\right)^{\frac{1}{2}} - \tfrac{1}{2}\left[1 + \frac{\chi}{\beta} - j_m\left(\frac{1+\beta}{\beta}\right)^{\frac{1}{2}}\right]^{\frac{1}{2}} - e^{-\chi} \tag{4.14}$$

in the limit as $\xi_e \to \infty$. The error in Eq. (4.14) is $O(\xi_e^{-1})$. The boundary condition for $\chi(t)$ is simply that as $t \to -\infty$ the solution must match the limiting behavior of the first transitional layer solution $Y(y)$ near $y = y_2$. After some algebra, this boundary condition is expressed as:

$$\lim_{t\to-\infty} \chi(t) = \chi_2 + (z_1 j^{\frac{1}{2}})^4 (C/At^2), \tag{4.15}$$

where

$$\chi_2 = \chi_1(\beta) + O(\xi_e^{-1/5}) \cong \chi_1(\beta). \tag{4.16}$$

This boundary condition alone is again sufficient to render the solution $\chi(t; \beta)$ unique. The actual family of solutions must again be obtained numerically. However, our main interests here concern the behavior of the solution for large t. As t increases, the magnitude of χ/β eventually becomes large. Equation (4.14) then takes on the limiting form given below:

$$j_m \frac{d^2\chi}{dt^2} = \frac{(1+\beta)^{\frac{1}{2}}}{4\chi^{\frac{1}{2}}}, \qquad \left(\frac{\chi}{\beta} \gg 1 \quad \text{assumed}\right). \tag{4.17}$$

The asymptotic solution for large t is then, by quadrature,

$$\lim_{t\to\infty} \chi(t; \beta) = \left[\frac{3}{4}\frac{(1+\beta)^{\frac{1}{2}}}{j_m^{\frac{1}{2}}} t + \chi_3(\beta)\right]^{4/3} \cong (1+\beta)^{\frac{1}{3}}\left(\frac{3}{4}\frac{t}{j_m^{\frac{1}{2}}}\right)^{4/3}, \tag{4.18}$$

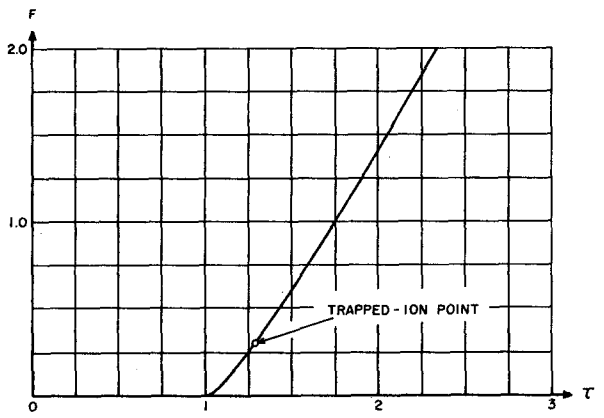

FIG. 2. Numerical solution for F vs τ, spherical case.

where $\chi_3(\beta)$ is expected to be $O(1)$ and can only be determined if the complete numerical solution for $\chi(t;\ \beta)$ is available. Equation (4.18) is essentially the Child–Langmuir formula. No calculation has been performed to determine $\chi_3(\beta)$.

In Fig. 1, the structure of the second transitional layer is also schematically sketched. No numerical calculation has been performed for $\chi(t;\ \beta)$, for we shall see that it is not important for our purposes.

Note that in both transitional-layer analyses the factor z^4 on the left-hand side of Eq. (2.3) has been approximated by a constant, z_1^4. Thus, no curvature effect is included.

Sheath Region

Beyond the second transitional layer, we come to the sheath region. We see from Eq. (4.17) that the number density of the electrons has become negligible by the time the second transitional layer is traversed. In the sheath region, therefore, there exist only ions. The curvature effect which had previously been neglected in the transitional-layer analysis must now be properly included. The proper governing equation under the condition that $\chi \gg 1$ is now

$$\frac{1}{\xi_e^2} z^2 \frac{d^2\chi}{dz^2} = \frac{j(1+\beta)^{\frac{1}{2}}}{4\chi^{\frac{1}{2}}}. \tag{4.19}$$

We again introduce new variables by

$$\chi = \left[\frac{j\xi_e^2(1+\beta)^{\frac{1}{2}}}{4}\right]^{\frac{4}{3}} F(\tau), \tag{4.20}$$

$$\tau = \frac{z}{z_2} = z\left(\frac{j}{j_m}\right)^{\frac{1}{4}}. \tag{4.21}$$

The equation for $F(\tau)$ is then

$$\tau^2 \frac{d^2F}{d\tau^2} = \frac{1}{F^{\frac{1}{2}}}. \tag{4.22}$$

The boundary condition is simply that, as $\tau \to 1$, $F(\tau)$ should match smoothly with the large t behavior of the second transitional layer solution, Eq. (4.18). After some algebra, this boundary condition is expressed as

$$\lim_{\tau\to 1} F(\tau) = (\tfrac{3}{2})^{4/3}(\tau - 1)^{4/3}. \tag{4.23}$$

This single boundary condition again renders $F(\tau)$ unique. The solution $F(\tau)$ has been numerically integrated and is plotted in Fig. 2, and tabulated in Table V. It is also schematically sketched in Fig. 1. Since it contains no parameters, it is therefore an universal curve. For large τ, it tends asymptotically to

$$\lim_{\tau\to\infty} F(\tau) = 1.9\tau - 2.7, \tag{4.24}$$

where the numerical coefficients are determined from the numerical solution.

At $z = 1$, $\tau = j/j_m$, we must impose the boundary condition that $\chi = \chi_p$. Thus,

$$\chi_p = [\tfrac{1}{4} j\xi_e^2(1+\beta)^{\frac{1}{2}}]^{\frac{4}{3}} F[\tau = (j/j_m)^{\frac{1}{4}}]. \tag{4.25}$$

Eq. (4.25) is the ion C–V characteristic for highly negative probes. When Eq. (4.25) is rewritten in dimensional form, we have

$$-\frac{\phi_p}{(eI_i)^{\frac{1}{3}}} = \left(\frac{m_i}{2eZ}\right)^{\frac{1}{3}} F(j^{\frac{1}{4}}/j_m^{\frac{1}{4}}),$$

which, in practical units, becomes

$$\frac{-\phi_p(\text{volts})}{[eI_i(\text{amperes})]^{\frac{1}{3}}} \cong 7.41 \times 10^3 \left(\frac{a}{Z}\right)^{\frac{1}{3}} F(j^{\frac{1}{4}}/j_m^{\frac{1}{4}}), \tag{4.26a}$$

or

$$\frac{-\phi_p(\text{volts})}{[eI_i(\text{milliamps})]^{\frac{1}{3}}} \cong 74.1 \left(\frac{a}{Z}\right)^{\frac{1}{3}} F(j^{\frac{1}{4}}/j_m^{\frac{1}{4}}), \tag{4.26b}$$

TABLE V. Universal functions, spherical case.

τ	$F(\tau)$	$\tau^{4/3}F(\tau)$	$j/j_m = \tau^2$
1.0	.00000	.00000	0.000
1.01	.00370	.00375	1.020
1.02	.00929	.00954	1.040
1.03	.01590	.01654	1.061
1.04	.02327	.02452	1.082
1.05	.03125	.03335	1.102
1.10	.07775	.08829	1.210
1.15	.13189	.15890	1.32
1.20	.19131	.24395	1.440
1.25	.25473	.34300	1.562
1.295[a]	.31456	.44401	1.677
1.30	.32135	.45593	1.690
1.50	.610	1.06	2.25
2.00	1.41	3.60	4.0
3.00	3.19	13.80	9.0
10.00	16.4	353.0	100.0

[a] Trapped-ion point.

where ϕ_p is the probe potential relative to infinity and a is the atomic weight of the ions. The important feature of Eq. (4.26) is that it is independent of ξ_e, N_∞, and T_e. In an experimental situation where ϕ_p and eI_i are measured, Eq. (4.26) gives immediately the value of j/j_m. If the value of β is somehow known so that the value of j_m can be obtained from Table III, the value of j corresponding to the measured value of I_i can be obtained.

The Trapped-Ion Criterion

Bernstein and Rabinowitz showed that for a given $\phi(r)$ distribution, the probe radius must be larger than a certain critical value in order to avoid the possibility that some particles may be trapped in effective potential wells. For a fixed probe radius, the trapped-ion possibility occurs when the probe potential reaches a critical value χ_c. The value of χ_c is defined as the value of χ_p for which the value of Q defined by

$$Q = \left[\frac{d}{dz}\left(\frac{1}{z}\frac{d\chi}{dz}\right)\right]_{z=1} \tag{4.27}$$

is zero. Using the sheath region solution, Eq. (4.20), we find that the condition $Q = 0$ is equivalent to

$$\left(\frac{dF}{d\tau} - \frac{1}{\tau F^{\frac{1}{2}}}\right)_{\tau=(j/j_m)^{\frac{1}{2}}} = 0. \tag{4.28}$$

We use subscript c to indicate this critical condition. From the numerical solution for F, we find this critical value of $(j/j_m)_c$ to be 1.677. Using this value of $(j/j_m)_c$ in Eq. (4.26), we have the following explicit trapped-ion criterion:

$$\frac{-\phi_p(\text{volts})}{[eI_i(\text{amperes})]^{\frac{2}{3}}} = 2.33 \times 10^3\left(\frac{a}{Z}\right)^{\frac{1}{3}}. \tag{4.29}$$

In an experimental situation, the above criterion can easily be applied.

When $j > j_c$, the region between $r = R$ and $r = R(j/j_c)^{\frac{1}{2}}$ may contain trapped ions. Since in the sheath region ions are already in excess any trapped ions simply serve to raise the value of χ_p above the value predicted by Eq. (4.25).

The $\beta \gg 1$ Case

A rigorous treatment of the $\beta \gg 1$ case would be rather complicated for the behavior of the solution will now depend critically on the ordering of the three large parameters ξ_e, β, and χ_p. We give only a qualitative discussion here.

For $\beta = O(1)$, the exact solution curve lies slightly above the quasineutral curve in the interval $0 < z < z_0$, crosses the quasineutral curve shortly after z_0, goes on to osculate the osculating line, and then follows the quasineutral curve from below until $z_1 - z = O(\xi_e^{-4/5})$ where it enters the first transitional layer. It is tacitly assumed that for $0 < z < z_1 - O(\xi_e^{-4/5})$, the quasineutral approximation is uniformly valid. However, when β becomes large, the distance between z_0 and z_1 is $O(\beta^{-\frac{1}{2}})$. Hence when $\beta^{\frac{1}{2}}\xi_e^{-4/5} = O(1)$, the osculating point of the solution, if such a point exists, will appear inside a new first transitional layer. Consequently, the analysis in the previous sections is valid only if $\beta^{\frac{1}{2}}\xi_e^{-4/5} \ll 1$.

The next point of interest is whether the solution curve always osculate the osculating line. Consider the case of $\chi_p = O(1)$, $\xi_e = O(1)$, and $\beta \to \infty$ so that $\chi/\beta \ll 1$. From Eq. (2.7) we see that the osculating line becomes vertical in this limit. Obviously no solution curve can osculate this line. Physical arguments (see Sec. 9) show that the solution shall simply intercept the "osculating line" and the point of interception must be identified as the body surface. Hence for the $\chi_p/\beta \ll 1$, $\beta \gg 1$ case, the C–V characteristic is simply, from Eq. (2.7),

$$j = \left(1 + \frac{\chi_p}{\beta}\right)\left(\frac{\beta}{1+\beta}\right)^{\frac{1}{2}}.$$

Mathematically, the important point to be noted is that the solution curve does not always osculate Eq. (2.7). The point is further discussed in Sec. 9 in the study of the limiting case of $\xi_e \to 0$.

V. POSITIVE AND INTERMEDIATELY NEGATIVE PROBE POTENTIALS

If we are willing to assume when the probe potential is positive that at infinity the electrons are mono-energetic with energy E_e and that the ions have a Maxwellian distribution function with temperature T_i, then the previous negative probe analysis can be applied directly, by simply changing certain subscripts and definitions. Using an asterisk to identify these variables, we have

$$\begin{aligned}
\chi_* &= \frac{e\phi}{KT_i} = -\chi\frac{T_e}{T_i}, \\
j_* &= \frac{I_e}{\pi R^2 N_\infty [2(KT_i + E_e)/m_e]^{\frac{1}{2}}}, \\
\beta_* &= \frac{E_e}{KT_i} = \frac{1}{\beta}\frac{E_e}{ZKT_e}\frac{E_i}{KT_i}, \\
\xi_{e*} &= \frac{R}{h_i} = R\left(\frac{4\pi N_\infty e^2}{KT_i}\right)^{\frac{1}{2}} = \xi_e\left(\frac{T_e}{T_i}\right)^{\frac{1}{2}},
\end{aligned} \tag{5.1}$$

where h_i is the ion Debye length and the definition for z remains unchanged. In Eq. (5.1), I_e is the total

electron particle current collected by the probe and m_e is the mass of an electron. All results obtained in the previous sections become valid for positive probe potentials if all variables are given the asterisk subscript. Note that $\beta_* \gg 1$ when we have hot electrons and cold ions.

When the probe potential is intermediately negative, the analysis given in Secs. III and IV must be modified. The major complication here is that n_e as given by Eq. (2.8) contains χ_p and therefore the quasineutral curve depends on χ_p. It is suggested that the same procedures used in Section IV can again be employed. The values of z_0, z_1, A, B, C, D, and z_2 are now dependent on χ_p and j. Thus we can expect no universal functions, and a separate calculation must be performed for each value of χ_p by assuming a value for j. Iteration procedure is then necessary to affirm the χ_p vs j relation.

VI. MASTER C–V DIAGRAMS

In an experimental situation, the measured current I is the net current defined by

$$I = e(I_e - I_i) \tag{6.1}$$

where I_e is the number of electrons collected by the probe per unit time. For negative probe potentials, I_e has been derived in Appendix I to be

$$I_e/I_{e\infty} = e^{-\chi_p}, \tag{6.2}$$

where

$$I_{e\infty} = \frac{\pi}{\Gamma(\frac{3}{2})} R^2 N_\infty \left(\frac{2KT_e}{m_e}\right)^{\frac{1}{2}} \tag{6.3}$$

and is easily identified as the random particle flux incident on a sphere in the absence of electric fields. We are now in a position to construct master C–V diagrams using results so far obtained.

From Eq. (4.25), we see that for a fixed value of χ_p, the value of j tends to j_m as $\xi_e \to \infty$. Hence j_m is the apparent "saturation" value for j in this limit.

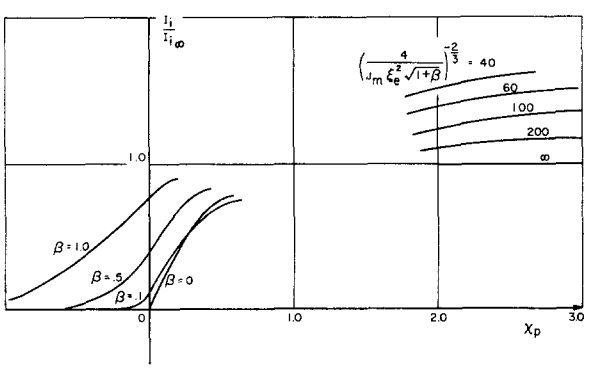

FIG. 3. Qualitative master C–V diagram for ions.

For fixed value of ξ_e, the value of j does not saturate as χ_p increases. With this in mind, let us define

$$I_{i\infty} = \pi R^2 N_\infty [2(ZKT_e + E_i)/m_i]^{\frac{1}{2}} j_m \tag{6.4}$$

as a reference value. Then from Eq. (2.6) we have

$$I_i/I_{i\infty} = j/j_m. \tag{6.5}$$

In Fig. 3, we plot $I_i/I_{i\infty}$ vs χ_p qualitatively using Eq. (3.2) for moderately negative potentials. Also plotted on the same diagram are curves for $I_i/I_{i\infty}$ for $\chi_p < 0$ and $\chi_p \gg 1$. For the $\chi_p < 0$ case, a calculation similar to that given in Appendix I shows that

$$I_i = \frac{\pi}{\Gamma(\frac{3}{2})} R^2 N_\infty \left(\frac{2KT_i}{m_i}\right)^{\frac{1}{2}} \exp\left(\frac{\chi_p Z T_e}{T_i}\right), \tag{6.6}$$

where T_i is the ion temperature. Matching the value of I_i from Eq. (6.6) at $\chi_p = 0$ with that given by Eq. (3.4), we have

$$E_i = \left[\frac{1}{\Gamma(\frac{3}{2})}\right]^2 KT_i, \tag{6.7}$$

which relates E_i to T_i. In other words, if T_i is the ion temperature based on Maxwellian distribution function, then Eq. (6.7) is the proper definition of E_i, so that the correct random current for the $\chi_p = 0$ case is obtained. The corresponding diagram for electrons can be constructed similarly.

Note in Fig. 3 that in the positive and moderately negative probe potential range, the curves are independent of ξ_e and are strongly dependent on β. In the highly negative probe potential range, the curves depend on the parameter $[j_m(1+\beta)^{\frac{1}{2}}\xi_e^2]^{\frac{1}{3}}$. Thus both cases are represented by single parameter curves. In the intermediate range of χ_p, therefore, we are led to expect two-parameter curves which are dependent on ξ_e and β separately.

A master C–V diagram for the highly negative potential case is presented in Fig. 4. To construct Fig. 4, we rewrite Eq. (4.25) as

$$\chi_p = [\tfrac{1}{4} j_m (1+\beta)^{\frac{1}{2}} \xi_e^2]^{\frac{2}{3}} \mathfrak{F}(I_i/I_{i\infty}), \tag{6.8}$$

where $\mathfrak{F}$ is defined by

$$\mathfrak{F}\left(\frac{I_i}{I_{i\infty}}\right) = \mathfrak{F}\left(\frac{j}{j_m}\right) = \left(\frac{j}{j_m}\right)^{\frac{2}{3}} F\left(\frac{j^{\frac{1}{2}}}{j_m^{\frac{1}{2}}}\right).$$

Thus $\{4/[j_m\xi_e^2(1+\beta)^{\frac{1}{2}}]\}^{\frac{1}{3}}\chi_p$ vs $I_i/I_{i\infty}$ is a universal curve and is plotted in the first quadrant. Equation (6.2) for the electron current is plotted in the third quadrant. In the second and fourth quadrants straight lines for constant $\{4/[j_m\xi_e^2(1+\beta)^{\frac{1}{2}}]\}^{\frac{1}{3}}$ and $I_{e\infty}/I_{i\infty}$ are drawn. Figure 4 can now be used to construct C–V diagrams for arbitrary but finite values of β and $\xi_e \gg 1$ for probes at highly negative probe

potentials. For any given value of large χ_p, we can obtain the corresponding values of $I_i/I_{i\infty}$ and $I_e/I_{i\infty}$ by following the dotted lines shown in Fig. 4 for illustrative purposes. The value of the floating potential at which $I_i = I_e$ can be obtained easily by applying graphical iteration. We see immediately from Fig. 4 that

$$\chi_p(\text{floating}) \cong \ln\left(\frac{I_{e\infty}}{I_{i\infty}}\right) = \ln\left[\frac{1}{j_m\Gamma(\frac{3}{2})}\left(\frac{m_i}{Zm_e(1+\beta)}\right)^{\frac{1}{2}}\right]$$

in the limit of $\xi_e \to \infty$ and its value decreases for lower values of ξ_e. Experimentally, if $I_i/I_{i\infty}$ (or j/j_m) is determined from Eq. (4.26) and if T_e is somehow known—such as from the slope of a ln I_e vs ϕ_e curve—then the value of $j_m(1+\beta)^{\frac{1}{2}}\xi_e^2$ can be found. If β is also known, the value of N_∞ can be deduced.

In the intermediate range of χ_p, for which neither Fig. 3 nor Fig. 4 is valid, we must in principle perform a separate analysis as was discussed in Sec. V. However, if we are willing to stretch the validity of Eq. (2.13) as an approximation for this χ_p range, then within this framework the probe surface is adjacent to the second transitional layer. For this case, Eq. (4.18) becomes an "approximate" ion C–V characteristic, if we replace t by $[1 - (j_m/j)^{\frac{1}{2}}]j\xi_e$. We obtain

$$\begin{aligned}\chi_p &= \{\tfrac{1}{4}[3(1+\beta)^{\frac{1}{4}}j^{\frac{1}{2}}\xi_e][(j/j_m)^{\frac{1}{2}} - 1] + \chi_3(\beta)\}^{4/3} \\ &= \{\tfrac{1}{4}[j(1+\beta)^{\frac{1}{2}}\xi_e^2\}^{\frac{2}{3}}\left[\frac{3}{2}\left[\left(\frac{j}{j_m}\right)^{\frac{1}{2}} - 1\right] + \frac{2\chi_3}{j^{\frac{1}{2}}(1+\beta)^{\frac{1}{4}}\xi_e}\right]^{4/3}. \qquad (6.9)\end{aligned}$$

For $(j/j_m)^{\frac{1}{2}} - 1 \gg \xi_e^{-1}$, Eq. (6.9) tends to Eq. (4.25) as it should. *Hence this inequality is the criterion for the validity of the highly negative probe potential results.*

Equation (6.9) suggests that the exact C–V expression for intermediate χ_p is most likely to be quite complicated and is therefore not expected to be useful for probe purposes.

VII. CYLINDRICAL PROBES

The analysis for the cylindrical probe case proceeds analogously. The governing equation is

$$\frac{1}{\xi_e^2} z^3 \frac{d}{dz}\left(z\frac{d\chi}{dz}\right) = n_i - n_e, \qquad (7.1)$$

where χ, z, and ξ_e are defined as before except that r and R are now the radial polar coordinate and the radius of the cylinder, respectively. The expression for n_i is given by Bernstein and Rabinowitz as:

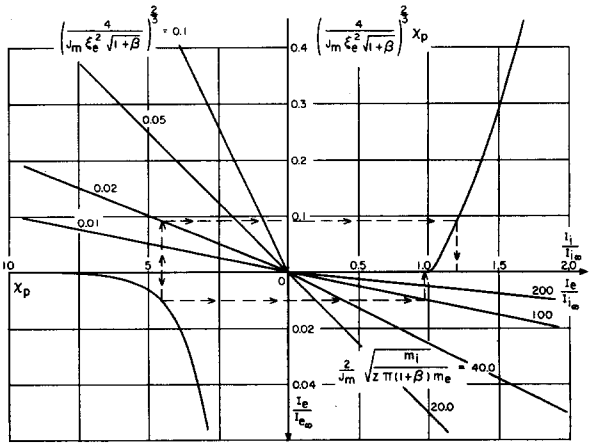

FIG. 4. Master C–V diagram, spherical case.

for $z \le z_0$,

$$n_i = 1 - \frac{1}{\pi}\sin^{-1}\left\{jz\left(\frac{1+\beta}{\chi+\beta}\right)^{\frac{1}{2}}\right\}, \qquad (7.2a)$$

for $z \ge z_0$,

$$n_i = \frac{1}{\pi}\sin^{-1}\left\{jz\left(\frac{1+\beta}{\chi+\beta}\right)^{\frac{1}{2}}\right\}, \qquad (7.2b)$$

where

$$j = \frac{I_i}{2RN_\infty[2(ZKT_e + E_i)/m_i]^{\frac{1}{2}}} \qquad (7.3)$$

and z_0 is defined as the value of z at which the solution curve osculates the following curve:

$$jz = (\chi+\beta)^{\frac{1}{2}}/(1+\beta)^{\frac{1}{2}}. \qquad (7.4)$$

In Eq. (7.3), I_i is the number of positive charges collected by the probe per unit length per unit time. All other symbols have the same meanings as before.

A simple calculation shows that

$$\chi_0 = \ln 2, \qquad jz_0 = \left(\frac{\ln 2 + \beta}{1+\beta}\right)^{\frac{1}{2}}. \qquad (7.5)$$

It is important to note that χ_0 is independent of β. Furthermore, jz_0 is finite even when $\beta = 0$ in contrast to the spherical case.

Moderately Negative Probe Potentials

On the probe surface, we have $n_e = \frac{1}{2}e^{-\chi_p}$ as before. Assuming again quasineutrality throughout the plasma and equating n_i and n_e at $z = 1$, we have, for $\chi_p \le \bar{\chi}_p$,

$$j = \left(\frac{\chi_p+\beta}{1+\beta}\right)^{\frac{1}{2}}\sin(\tfrac{1}{2}\pi e^{-\chi_p}), \qquad (7.6)$$

which is the ion C–V characteristic for moderate probe potentials. The error here is $O(\xi_e^{-2})$ and $\bar{\chi}_p(\beta)$

TABLE VI. The values of $\bar{\chi}_p$, $j(\bar{\chi}_p)$, χ_1, and j_m for the cylindrical case.

β	0	0.1	0.5	1.0	2.0	5.0	10.0	∞
$\bar{\chi}_p$	0.61	0.61	0.41	0.23	0.12	0.05	0.02	0
$(\bar{\chi}_p)$	0.59	0.61	0.67	0.74	0.83	0.91	0.96	1.0
χ_1	0.99	0.96	0.89	0.83	0.78	0.73	0.71	ln 2
jz_1 or j_m	0.92	0.92	0.92	0.94	0.95	0.98	0.99	1.00

is again the upper limit of χ_p beyond which the quasineutral assumption breaks down near the probe. The determination of $\bar{\chi}_p$ is analogous to the spherical case. Table VI gives $\bar{\chi}_p$ and $j(\bar{\chi}_p)$ vs β.

For the highly negative probe potential case, we have $n_e = e^{-\chi}$. For $\xi_e \gg 1$ we have $n_i = n_e + O(\xi_e^{-2})$ which yields the quasineutral curve:

$$jz = \left(\frac{\chi + \beta}{1 + \beta}\right)^{\frac{1}{2}} \sin(\pi e^{-\chi}). \tag{7.7}$$

We again denote by χ_1, z_1 the point where the quasineutral curve doubles back on itself. From simple calculus we have the following equations for χ_1 and z_1:

$$\tan(\pi e^{-\chi_1}) = 2(\chi_1 + \beta)\pi e^{-\chi_1}, \tag{7.8}$$

$$jz_1 = \left(\frac{\chi_1 + \beta}{1 + \beta}\right)^{\frac{1}{2}} \sin(\pi e^{-\chi_1}).$$

Table VI also gives the values of χ_1 and j_m where j_m is defined analogously as the spherical case

$$j_m = jz_1. \tag{7.9}$$

We side-step the transitional layers and proceed directly to the sheath region for the highly negative probe potential case. The governing equation is found to be

$$\frac{1}{\xi_e^2} z^2 \frac{d}{dz}\left(z \frac{d\chi}{dz}\right) = \frac{j(1 + \beta)^{\frac{1}{2}}}{\pi \chi^{\frac{1}{2}}} \tag{7.10}$$

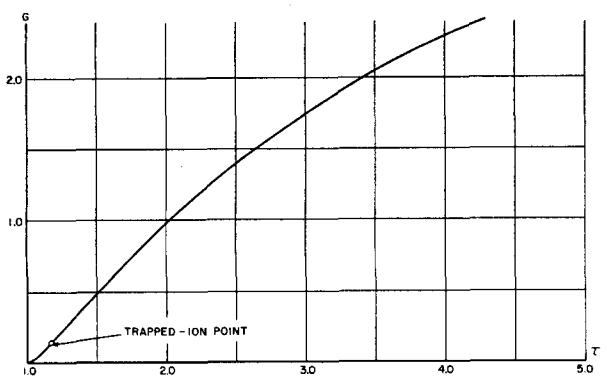

FIG. 5. Numerical solution for $G(\tau)$, cylindrical case.

where we have approximated

$$\sin^{-1}\{jz[(1 + \beta)/(\chi + \beta)]^{\frac{1}{2}}\}$$

by $jz[(1 + \beta)/\chi]^{\frac{1}{2}}$ and have neglected n_e in comparison to it. We now let

$$\chi = \left(\frac{j^2\xi_e^2(1 + \beta)^{\frac{1}{2}}}{j_m\pi}\right)^{\frac{2}{3}} G(\tau), \tag{7.11a}$$

$$\tau = z/z_1 = zj/j_m. \tag{7.11b}$$

Then the equation for $G(\tau)$ is

$$\tau^2 \frac{d}{d\tau}\left(\tau \frac{dG}{d\tau}\right) = \frac{1}{G^{\frac{1}{2}}} \tag{7.12}$$

and the appropriate boundary condition is, analogous to Eq. (4.23),

$$\lim_{\tau \to 1} G(\tau) = (\tfrac{3}{2})^{4/3}(\tau - 1)^{4/3}. \tag{7.13}$$

Hence $G(\tau)$ is also a universal function. Evaluating Eq. (7.11a) at the probe surface, we have

$$\chi_p = \left(\frac{j\xi_e^2}{\pi}(1 + \beta)^{\frac{1}{2}}\right)^{\frac{2}{3}}\left(\frac{j}{j_m}\right)^{\frac{2}{3}} G\left(\frac{j}{j_m}\right). \tag{7.14}$$

Alternatively, we have

$$\left(\frac{\pi}{j_m(1 + \beta)^{\frac{1}{2}}\xi_e^2}\right)^{\frac{2}{3}} \chi_p = \left(\frac{j}{j_m}\right)^{4/3} G\left(\frac{j}{j_m}\right), \tag{7.15}$$

or

$$-\frac{\phi}{(eI_iR)^{\frac{2}{3}}} = \left(\frac{2m_i}{Ze}\right)^{\frac{1}{3}}\left(\frac{j}{j_m}\right)^{\frac{2}{3}} G\left(\frac{j}{j_m}\right),$$

which in practical units becomes

$$\frac{-\phi(\text{volts})}{[eI_iR(\text{amperes})]^{\frac{2}{3}}} = 1.19 \times 10^4\left(\frac{a}{Z}\right)^{\frac{1}{3}}\left(\frac{j}{j_m}\right)^{\frac{2}{3}} G\left(\frac{j}{j_m}\right). \tag{7.16}$$

Figure 5 shows $G(j/j_m)$ vs j/j_m. It should be noticed that for fixed ξ_e the value of j/j_m increases rapidly for increasing χ_p in contrast to the saturation-like type behavior normally expected. For fixed χ_p, the value of j/j_m again tends to 1.0 as ξ_e increases.

The trapped-ion condition for the cylindrical case can be shown to be

$$\left(\frac{dG}{d\tau} - \frac{1}{2\tau^2 G^{\frac{1}{2}}}\right)_{\tau = j/j_m} = 0. \tag{7.17}$$

From the numerical solution, the value of $(j/j_m)_c$ is found to be 1.167. Using this value of $(j/j_m)_c$ in Eq. (7.16), we have explicitly the following trapped-ion criterion:

$$\frac{-\phi(\text{volts})}{[eI_iR(\text{amperes})]^{\frac{2}{3}}} = 1.74 \times 10^3\left(\frac{a}{Z}\right)^{\frac{1}{3}}. \tag{7.18}$$

TABLE VII. Universal functions, cylindrical case.

$\tau = j/j_m$	$G(\tau)$	$\tau^{2/3}G(\tau)$	$\tau^{4/3}G(\tau)$
1.00	.00000	.00000	.00000
1.01	.00369	.00371	.00373
1.02	.00922	.00934	.00946
1.03	.01569	.01601	.01633
1.04	.02284	.02345	.02407
1.05	.03052	.03152	.03257
1.06	.03861	.04014	.04173
1.08	.05579	.05873	.06182
1.10	.07400	.07885	.08403
1.12	.09298	.10027	.10814
1.14	.11255	.12282	.13403
1.16_a	.13258	.14637	.16159
1.20	.17363	.19608	.22142
1.50	.48994	.64200	.84126

[a] Trapped-ion point.

In Table VII, $G(\tau)$, $\tau^{2/3}G(\tau)$ and $\tau^{4/3}G(\tau)$ are tabulated for $1.0 < \tau < 1.5$.

VIII. COMPARISON WITH EXISTING WORKS

The main features of the potential distribution about the probe were clearly identified by Langmuir. From physical arguments he concluded that the plasma was quasineutral outside a thin sheath region in which one type of charged particles dominates. The numerical solutions of Allen, Boyd, and Reynolds and Bernstein and Rabinowitz confirmed and displayed this feature graphically. The present theory in essence formalizes the original concepts of Langmuir by using the more rigorous formulation of Bernstein and Rabinowitz. For $\xi_e \gg 1$ and $(j/j_m)^{\frac{1}{2}} - 1 \gg \xi_e^{-1}$, we find that the electric potential distribution consists of a quasineutral region far from the probe, a sheath region adjacent to the probe and two thin transitional layers which serve to join the two regions. The transitional layers' thicknesses are of $O(\xi_e^{-4/5})$ and $O(\xi_e^{-1})$, respectively, and the sheath region thickness is $O[(j/j_m)^{\frac{1}{2}} - 1]$.

The so-called sheath criterion originated by Bohm, which states that the potential at the edge of the sheath is approximately $\frac{1}{2}KT$ where T is the temperature of the repelled particles, can now be interpreted in a new light. For a given temperature T of the repelled particles, the majority of these particles has kinetic energy of the order of $\frac{1}{2}KT$. When the probe potential is larger than $KT/2e$, only a small fraction of the repelled particles is allowed to reach the probe surface and an imbalance of quasi-neutrality results near the probe to form the sheath. When the probe potential is smaller than $KT/2e$, the majority of the repelled particles can still reach the probe surface so that quasineutrality can be maintained throughout the plasma. This interpretation is consistent with our conclusion in Sec. III that for $\chi_p \leq \tilde{\chi}_p$ no sheath exists in the plasma.

The value of n_i near the probe surface shows an unexpected behavior for large χ_p. In the sheath region, while n_e decreases rapidly, the value of n_i actually tends to increase toward the probe. This is purely a geometric effect since all the ions passing through the sheath edge are now being squeezed together. In the rather academic limit of $j/j_m \gg 1$, the value of n_i on the probe surface can actually exceed unity.

When $\beta \gg 1$, no limiting analysis is presented here. From Eq. (2.4) we can conclude immediately that n_i is independent of the potential distribution when $\beta \gg \chi_p$. Physically, this means that the random kinetic energy of the ions is so great that the presence of the electric field is not felt by the ions. The n_e distribution, however, is strongly dependent on $\chi(z)$. Thus, quasineutrality becomes difficult to maintain, for in a figurative sense the ions refuse to cooperate. For example, the value of n_i at $z = 1$ is $\frac{1}{2}$ in the limit of $\beta \gg \chi_p$ but the value of n_e is $\frac{1}{2}e^{-\chi_p}$ always. Thus, even when χ_p is moderately negative, quasineutrality must break down near the probe surface. This is substantiated by the fact that when $\beta \to \infty$, $\tilde{\chi}_p$ tends to zero. This is one of the many reasons why the $\beta \gg 1$ limiting case must be viewed separately from the rest.

In the $\beta \to 0$ limit, the model of Bernstein and Rabinowitz reduces identically to that of Allen, Boyd, and Reynolds for the spherical case. For the cylindrical case, the two theories disagree formally. The disagreement can be traced to the assumption adopted by Bernstein and Rabinowitz that the ion distribution function is a function of E_i only and is independent of the angular momentum J, which is defined as $m_i r^2 \dot{\theta}$ where $\dot{\theta}$ is the angular velocity of an ion with respect to the probe. Following Bernstein and Rabinowitz, we write

$$E_i = \tfrac{1}{2}m_i(\dot{r}^2 + r^2\dot{\theta}^2),$$

where $\dot{r}$ is the radial velocity of the ions. Assuming equipartition of kinetic energy at large r, we have

$$E_i = m_i r^2 \dot{\theta}^2 = J^2/m_i r^2 \tag{8.1}$$

or $J^2 = E_i m_i r^2$. In the limit of cold ions, $E_i \to 0$, the value of J at $r = \infty$ becomes indeterminate. If we assume that at $r = \infty$ all values of J are possible, we obtain Eq. (7.2) which was obtained by Bernstein and Rabinowitz. If we assume that as $E_i \to 0$, the only possible J is zero, so that the ion distribution function has a delta function behavior at $J = 0$, we can recover the equations given by

Allen *et al.* from the kinetic model of Bernstein and Rabinowitz. This subtle nonuniformity in the $\beta \to 0$ limit is an excellent example of how an assumed form of the distribution function can affect macroscopic results.

In reality, the radially inward part of the ion distribution function is supposed to be specified at $r = O(l) \gg R$. Then under the mono-energetic assumption, we have, from Eq. (8.1),

$$J = O[l(m_i E_i)^{\frac{1}{2}}]$$

and the distribution function for ions should be essentially zero for J larger than this value.

For a given net current collected by the probe, an Ohmic potential drop must occur between $r = \infty$ and $r = l$. Assuming the plasma *far from the probe* satisfies the simple Ohm's Law with a constant conductivity σ, this potential drop can be shown to be of $O(R/l)^2$ for the spherical case. For the cylindrical case, the corresponding calculation shows that this Ohmic drop is not bounded. This result suggests that the length of the cylinder is important and factors such as $\ln (l/L)$ are to be expected where L is the length of the cylinder.

In the continuum limit, the collision-dominated Langmuir probe problem for a weakly ionized plasma has been treated extensively by Su and Lam[5] and Cohen.[6] The corresponding problem for a flowing plasma is treated by Lam.[7] The collisionless probe problem in a flowing plasma, stimulated by satellite–ionosphere interaction data, has received considerable interest[8] in recent years. The boundary-layer-type analysis, which has proved successful in the large ξ_e limit for the present work as well as in Refs. 5–7, has been applied to this case by Lam and Greenblatt.[9]

IX. DISCUSSION

Within the collisionless framework and the assumption of mono-energetic ions, the present work is a consistent asymptotic analysis under the restriction that the probe size is large compared to the Debye-length. In Sec. III, we have shown that when $\bar{\chi}_p > \chi_p \geq 0$, the plasma is quasineutral to $O(\xi_e^{-2})$ throughout and the ion C–V diagram can be constructed without precise knowledge of the spatial potential distribution. When $\chi_p \gg 1$, we showed in Sec. IV that quasineutrality fails near the probe surface where a sheath region exists. *The ion* C–V *diagram for this case depends only on the detailed spatial potential distribution in the sheath region.* The analysis of the quasineutral region and the transitional layers were presented merely to demonstrate that a continuous and uniformly valid approximate solution can be constructed if desired and also to furnish the value of j_m. In the cylindrical case the transitional layer analysis was omitted.

The structure of the potential distribution $\chi(z)$ for the $\chi_p \gg 1$ case allows the following physical interpretation. In the region between $r = \infty$ and $r = r_0 = R/z_0$, the ions travel in a relatively weak electric field. Some ions travelling in this region never strike the probe. Combining Eqs. (2.6) and (4.3b), we have

$$I_i = N_\infty \left(\frac{2E_i}{m_i}\right)^{\frac{1}{2}} \left\{\pi \left[r_0 \left(1 + \frac{\chi_0}{\beta}\right)^{\frac{1}{2}}\right]^2\right\}, \qquad (9.1)$$

which is the classical free molecular value for the particle flux incident on a sphere of radius $r_0[1 + (\chi_0/\beta)]^{\frac{1}{2}}$ in a gas with density N_∞ and kinetic energy E_i. Thus $r_0[1 + (\chi_0/\beta)]^{\frac{1}{2}}$ is the apparent capture radius of the probe for the ions far from the probe. Any ion at infinity which would have struck this apparent sphere if it had followed a linear trajectory, will enter the $r = r_0$ sphere by the action of the electric field. Upon entering the $r = r_0$ sphere, the ions spiral inward toward the probe. For $\xi_e^2 \gg 1$, the electron number density n_e follows closely that of the ions, n_i. At $r = r_1 = R/z_1 < r_0$, however, the local potential becomes sufficiently high so that the majority of the electrons is turned back. Thus r_1 is properly interpreted as the edge of the sheath. In the $R < r < r_1$ region, the electron number density becomes negligible, and the electric field is strong. The energy gained by the ions is essentially converted to radial kinetic energy in the $r_0 > r > r_1$ region.

Most of the above physical picture is well known and can be traced to various papers by Langmuir. It is important to note, however, that $r_0 \geq R$ always from these arguments.

We are now in a position to discuss the Langmuir probe problem for arbitrary ξ_e. To this end let us define

$$\eta = j^{\frac{1}{3}} z, \qquad i = j\xi_e^2. \qquad (9.2)$$

Then Eqs. (2.3), (2.4), and (2.13) together give

$$\frac{1}{i}\,\eta^4 \frac{d^2\chi}{d\eta^2} = H(\eta, \chi; \beta), \qquad (9.3)$$

[8] F. Hohl and G. Wood, *Rarefied Gas Dynamics*, edited by J. A. Laurmann (Academic Press Inc., New York, 1963), pp. 45–64.

[9] S. H. Lam and M. Greenblatt, in *Rarefied Gas Dynamics*, edited by J. de Leeuw (Academic Press Inc., New York, 1965).

where

$$H = \tfrac{1}{2}\left(1 + \frac{\chi}{\beta}\right)^{\frac{1}{2}} \pm \tfrac{1}{2}\left[1 + \frac{\chi}{\beta} - \eta^2\left(\frac{1+\beta}{\beta}\right)^{\frac{1}{2}}\right]^{\frac{1}{2}} - e^{-\chi}, \tag{9.4}$$

and the plus and minus signs are to be used for $\eta \leq \eta_0 = jz_0$ and $\eta \geq \eta_0 = jz_0$, respectively. Note that Eq. (9.3) is a second order ordinary nonlinear differential equation. We suppose that the values of i, β, and ξ_e are known. Under this formulation the boundary condition becomes

$$\chi(\eta = 0) = 0. \tag{9.5}$$

Supposing that Eq. (9.5) alone renders the solution unique, then by evaluating $\chi(\eta)$ at the probe surface, $\eta = i^{\frac{1}{2}}/\xi_e$, we have

$$\chi(\eta = i^{\frac{1}{2}}/\xi_e) = \chi_D. \tag{9.6}$$

Equation (9.6) yields the value of χ_D corresponding to the set of values of i, β, and ξ_e.

The important question which immediately arises is whether the problem as stated above is well posed. Since $\eta = 0$ is a singular point of Eq. (9.3), let us first analyze the behavior of the solution $\chi(\eta)$ near $\chi = 0$, $\eta = 0$. We begin by expanding Eq. (9.4a) about the origin to obtain:

$$H \cong \chi\left(1 + \frac{1}{2\beta}\right) - \tfrac{1}{4}\eta^2\left(\frac{1+\beta}{\beta}\right)^{\frac{1}{2}},$$

so that Eq. (9.3) becomes for $\chi/\beta \ll 1$, $\eta \ll 1$,

$$\frac{1}{i}\,\eta^4\,\frac{d^2\chi}{d\eta^2} \cong \chi\left(1 + \frac{1}{2\beta}\right) - \tfrac{1}{4}\eta^2\left(\frac{1+\beta}{\beta}\right)^{\frac{1}{2}}, \tag{9.7}$$

which is a linear differential equation. In arriving at Eq. (9.7) we have assumed β to be finite and that $\chi_s > \chi$, $\eta_s > \eta$, where subscript s indicates the osculating point between the solution and Eq. (2.7). We can split the solution $\chi(\eta)$ into two parts by writing

$$\chi = \chi_1(\eta) + \chi_2(\eta),$$

where χ_1 is the homogeneous and χ_2 is the particular solution of Eq. (9.7). For $\eta \ll 1$, the homogeneous solution χ_1 has the form:

$$\begin{aligned}\chi_1 &= S(\eta)\,\exp\left\{-\frac{[i(1+1/2\beta)]^{\frac{1}{2}}}{\eta}\right\} \\ &= S(\eta)\,\exp\left[-\left(1 + \frac{1}{2\beta}\right)^{\frac{1}{2}}\frac{r}{h_e}\right],\end{aligned} \tag{9.8}$$

where $S(\eta)$ is an analytic function of η. The exponential factor in Eq. (9.8) is referred to by Bernstein and Rabinowitz as "subdominal."

When $\xi_e \gg 1$, so that $r \gg h_e$ always, these subdominal terms are always exponentially small. In the analysis given in Secs. III and IV, they are tacitly suppressed and the single boundary condition given by Eq. (9.5) alone is sufficient to render the solution $\chi(\eta)$ unique. When ξ_e is $O(1)$ or smaller, however, these subdominal terms will become important and Eq. (9.5) alone is no longer sufficient. To clarify the situation it is advantageous to consider the limiting case of $i \to 0$. Eq. (9.3) yields immediately

$$\chi = C_1\eta + C_2. \tag{9.9}$$

Applying boundary condition Eq. (9.5), we have $C_2 = 0$ but C_1 remains unspecified. The solution given by Eq. (9.9) is valid only for $\eta \gg i$. For $\eta = O(i^{\frac{1}{2}})$ [or $r = O(h_e)$], a boundary layer of quasi-neutrality exists near $\eta = 0$ similar to the small probe solution of Su and Lam.[5] To determine C_1, we recall that the solution curve must be such that $H(\chi, \eta; \beta)$, as defined by Eqs. (9.4), must remain real. Hence

$$1 + \frac{\chi}{\beta} \geq \eta^2\left(\frac{1+\beta}{\beta}\right)^{\frac{1}{2}}. \tag{9.10}$$

Since Eq. (9.9) is a straight line, the solution *cannot* osculate the osculating line which is given by

$$1 + \frac{\chi}{\beta} = \eta^2\left(\frac{1+\beta}{\beta}\right)^{\frac{1}{2}}. \tag{9.11}$$

Hence for any finite C_1, the solution must intercept Eq. (9.11) at some point (χ_s, η_s). From our previous physical interpretation of the osculating point, however, we must require $\eta_s \geq \eta_D = i^{\frac{1}{2}}/\xi_e$. Hence we conclude

$$\eta_s = \eta_D = i^{\frac{1}{2}}/\xi_e = j^{\frac{1}{2}},\ \chi_s = \chi_D,\ C_1 = \chi_D/j^{\frac{1}{2}}. \tag{9.12}$$

Substituting Eqs. (9.12) into Eq. (9.11), we have

$$j = \left(\frac{\beta}{1+\beta}\right)^{\frac{1}{2}}\left(1 + \frac{\chi_D}{\beta}\right) \tag{9.13}$$

which is the small spherical probe ion C–V relation originally derived by Langmuir and Mott-Smith.[1]

The potential distribution $\chi(\eta)$ for fixed χ_D and arbitrary i can now be seen qualitatively as shown in Figure 6. When $i \to 0$, the solution is a straight line as was discussed. When $i = i_s \ll 1$, the solution is essentially a straight line except that it barely osculates the osculating line at the probe. In this range of i, the negative sign in Eq. (9.4) is disregarded, and Eq. (9.13) is the appropriate C–V relation. When $i_s < i = O(1)$, the osculating point η_s becomes almost identical to η_0, and the solution is

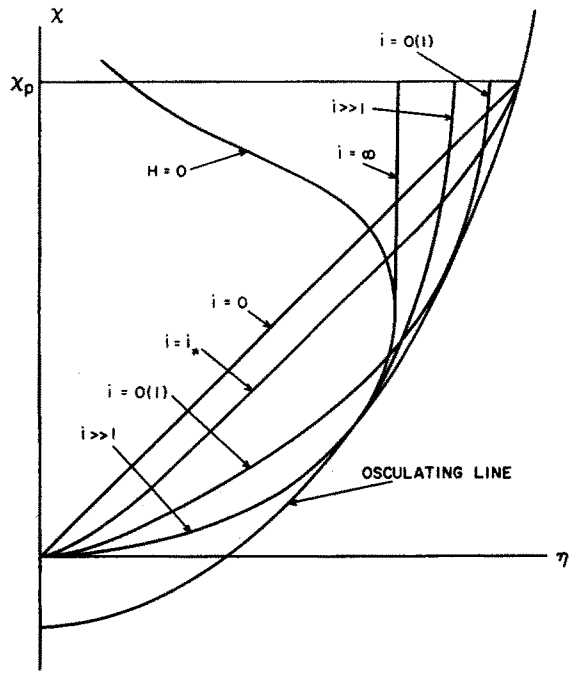

FIG. 6. Qualitative behavior of $\chi(\eta)$ for arbitrary values of i.

well approximated by the $H = 0$ quasineutral curve until $\eta \cong \eta_1$, beyond which the solution curve proceeds on its own. When $i \to \infty$, the solution curve becomes vertical at $\eta = \eta_1$. Since at the probe $\eta = j$, we see that the value of j for arbitrary β and ξ_e always lies in the range

$$j_m = \eta_1^2 \leq j \leq \left(\frac{\beta}{1+\beta}\right)^{\frac{1}{2}}\left(1 + \frac{\chi_p}{\beta}\right)$$

for highly negative probes.

ACKNOWLEDGMENTS

The author acknowledges Dr. I. Bernstein and Dr. F. Chen of the Princeton Plasma Physics Laboratory for the many discussions during the course of the work. This study was supported by the U. S. Air Force Office of Scientific Research Grant AF-AFOSR-112-63.

APPENDIX I. THE DISTRIBUTION FUNCTION AND NUMBER FLUX OF THE REPELLED PARTICLES

Let f be the distribution function of the repelled particles so that the number density N is given by

$$N = \int f \, d^3v \tag{A1}$$

and the mean velocity $\mathbf{V}$ is given by

$$\mathbf{V} = \frac{1}{N}\int f\mathbf{v} \, d^3v. \tag{A2}$$

Since the particles move without collisions in a conservative central force field, we have

$$f = f(E, J), \tag{A3}$$

where E is the sum of kinetic energy and (electric) potential energy and J is the angular momentum of a particle. Following Bernstein and Rabinowitz, Eqs. (A1) and (A2) become, for spherically symmetric f,

$$N = \frac{2\pi}{(mr)^2}\int \frac{fJ \, dE \, dJ}{[2m(E + Ze\phi) - J^2/r^2]^{\frac{1}{2}}}, \tag{A4}$$

$$\mathbf{V} = -\frac{\mathbf{e}_r}{N}\frac{2}{m^3r^2}\int fJ \, dE \, dJ, \tag{A5}$$

where Z is the charge number of the repelled particles. To proceed further, we must specify $f(E, J)$ and the appropriate regions of integration. We first note that the kinetic energy contributed by the radial component of the particle velocity is $E + Ze\phi - J^2/2mr^2$. At any fixed value of r, we require that this radial kinetic energy be positive. Thus

$$J^2 \leq 2mr^2[E + Ze\phi]. \tag{A6}$$

In Fig. 7, Eq. (A6) rules out the shaded region. At the same value of r, some particles there will travel inward and eventually strike and be absorbed by the probe. For these particles, their E and J^2 must be related such that when they arrive at $r = R$ their radial kinetic energy is positive. This condition requires

$$J^2 \leq 2\pi R^2[E + Ze\phi_p]. \tag{A7}$$

Equation (A7) divides the remaining region in Figure 7 into Regions C and D. Particles in Region C are those that will never strike the probe, while particles in Region D are those that are on their way to strike the probe. Hence we have $f = f_\infty$ in Region C and $f = \frac{1}{2}f_\infty$ in Region D where f_∞ is the distribution

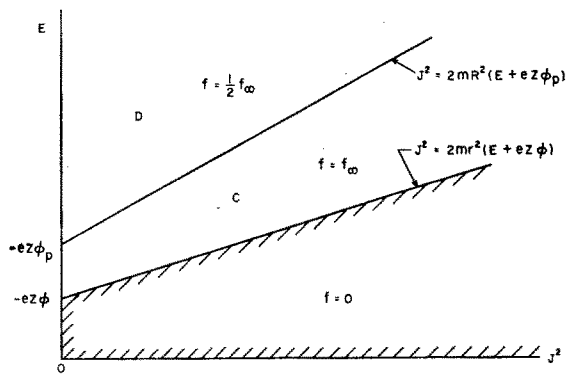

FIG. 7. Repelled particle distribution function in the E–J^2 plane.

function at infinity. The regions of integration for Eqs. (A4) and (A5) can be shown to be C + D and D, respectively.

We now assume f_∞ to be Maxwellian:

$$f_\infty = \frac{m(2m)^{\frac{1}{2}}}{4\pi\Gamma(\frac{3}{2})}\frac{N_\infty}{(KT)^{\frac{3}{2}}}e^{-E/KT}, \qquad \text{(A8)}$$

$$\Gamma(\tfrac{3}{2}) = \tfrac{1}{2}\pi^{\frac{1}{2}},$$

where N_∞ is the number density of the particles in question at infinity. Equation (A4) becomes

$$\frac{N}{N_\infty} = \frac{1}{2\Gamma(\frac{3}{2})}\left\{\int_{C+D}\frac{e^{-E/KT}\,d(J^2/2mr^2)\,d(E/KT)}{\{KT[E + Ze\phi - J^2/2mr^2]\}^{\frac{1}{2}}} - \tfrac{1}{2}\int_D \frac{e^{-E/KT}\,d(J^2/2mr^2)\,d(E/KT)}{\{KT[E + Ze\phi - J^2/2mr^2]\}^{\frac{1}{2}}}\right\}.$$

Integrating with respect to $J^2/2mr^2$ first, we have

$$\frac{N}{N_\infty} = \frac{1}{\Gamma(\frac{3}{2})}\left\{\int_\chi^\infty e^{-\xi}(\xi-\chi)^{\frac{1}{2}}\,d\xi - \tfrac{1}{2}\int_{\chi_p}^\infty e^{-\xi}\left\{(\xi-\chi)^{\frac{1}{2}} - \left[(\xi-\chi) - \frac{R^2}{r^2}(\xi-\chi_p)\right]^{\frac{1}{2}}\right\}d\xi\right\}, \qquad \text{(A9)}$$

where $\chi = -Ze\phi/KT$ and ξ is the dummy integration variable for E/KT. Defining $g(\lambda)$ by

$$g(\lambda) = \int_\lambda^\infty \xi^{\frac{1}{2}}e^{-\xi}\,d\xi, \qquad \text{(A10)}$$

and noting that $g(0) = \Gamma(\frac{3}{2})$, Eq. (A9) becomes, after some rearrangement,

$$\frac{N}{N_\infty} = e^{-\chi}\left(1 - \frac{1}{2g(0)}\left\{g(\chi_p-\chi) - (1-z^2)^{\frac{1}{2}}g\left(\frac{\chi_p-\chi}{1-z^2}\right)\cdot\exp\left[z^2\left(\frac{\chi_p-\chi}{1-z^2}\right)\right]\right\}\right) \qquad \text{(A11)}$$

which is the first desired result.

Using Eqs. (A8) in (A5), we can integrate to give

$$\mathbf{V} = -(\mathbf{e}_r)\frac{R^2}{r^2}\frac{N_\infty}{N}\left(\frac{KT}{2m}\right)^{\frac{1}{2}}\frac{1}{\Gamma(\frac{3}{2})}e^{-\chi_p}. \qquad \text{(A12)}$$

The total number of particles absorbed by the probe per second, I, is then given by

$$I = 4\pi r^2 N\mathbf{V}\cdot(-\mathbf{e}_r) = \frac{\pi R^2 N_\infty}{\Gamma(\frac{3}{2})}\left(\frac{2KT}{m}\right)^{\frac{1}{2}}e^{-\chi_p} \qquad \text{(A13)}$$

which is the second desired result.

If the electrons are the repelled particles, then $\phi < 0$ $Z = 1$, $m = m_e$, and $T = T_e$. If ions are the repelled particle, then $Z = Z$, $m = m_i$, and $T = T_i$.